NJC

Accepted Manuscript

ROYAL SOCIETY OF CHEMISTRY

www.rsc.org/njc

ARTICLE TYPE

Effect of 1,3-adamantane bridging units within the surrounding macrocycle of squaraine rotaxanes

Carleton G. Collins,[a] Andrew T. Johnson,*[b] Richard D. Connell,[a] Ruth A. Nelson,[b] Ivan Murgu,[a] Allen G. Oliver,[a] and Bradley D. Smith*[a]
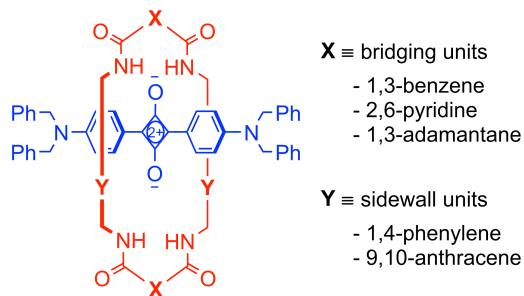
A systematic comparison of empty tetralactam macrocycles containing 1,3-benzenedicarboxamide, 2,6-pyridinedicarboxamide, and 1,3- adamantanedicarboxamide bridging units finds that macrocycles with adamantyl bridging units exhibit weaker non-covalent affinity for an encapsulated guest. In the case of
10 interlocked squaraine rotaxanes with macrocycles containing phenylene sidewalls, the structural change induced by the adamantyl bridging units produces a more loosely held rotaxane co-conformation that diminishes the ability of the surrounding macrocycle to protect the encapsulated squaraine dye from attack by nucleophiles. In the case of squaraine rotaxanes with macrocycles containing anthracene sidewalls, there is no obvious change in rotaxane co-conformation. But there is a difference with the
15 corresponding squaraine rotaxane endoperoxide, namely a significantly slower rate of cycloreversion and oxygen release. A series of molecular dynamics simulations provides reasons for the differences in co-conformational mobility. The overall result is a new set of structural strategies to control the chemical and photophysical properties of luminescent squaraine rotaxanes.

Introduction

20 In 2005, we reported the first preparation of squaraine rotaxanes (SR), interlocked molecules that permanently encapsulate a deep-red fluorescent squaraine dye inside a Leigh-type tetralactam macrocycle.[1,2] Over the intervening years we have examined a range of structural variants,[3-5] and using the improved insight we
25 have developed a series of high performance fluorescent molecular probes for different types of biological imaging applications.[6-10] We have also discovered a squaraine rotaxane endoperoxide (SREP) system that is capable of undergoing a thermally-activated singlet oxygen release reaction that emits
30 light.[11-13] In most of these structural studies, we have kept the core of the SR structure fairly constant. With regard the surrounding tetralactam macrocycle, we have primarily focused on versions that incorporate either 1,4-diaminomethylphenylene or 9,10-diaminomethylanthracene sidewalls. Likewise, the two
35 bridging units within the surrounding macrocycle have been either 1,3-benzenedicarboxamide or 2,6-pyridinedicarboxamide units (Scheme 1). We have learned that relatively small structural differences in the macrocycle structure can lead to substantial changes in SR molecular dynamics and photophysical
40 properties.[14,15] By improving our understanding of these structure/activity relationships we are able to fine tune the molecular properties of these fascinating compounds and optimize their functional performance.

Here, we report the effect of having two 1,3-
45 adamantanedicarboxamide bridging units within the tetralactam macrocycle.[16-18] We make a systematic comparison of molecules

Scheme 1

X ≡ bridging units
- 1,3-benzene
- 2,6-pyridine
- 1,3-adamantane

Y ≡ sidewall units
- 1,4-phenylene
- 9,10-anthracene

with macrocycles containing 1,3-benzenedicarboxamide, 2,6-
50 pyridinedicarboxamide, and 1,3-adamantanedicarboxamide bridging units (hereafter abbreviated as isophthaloyl, pyridyl, and adamantyl respectively) and find that empty macrocycles with adamantyl bridging units exhibit weaker non-covalent affinity for an encapsulated guest. In the case of interlocked SR molecules
55 with macrocycles containing phenylene sidewalls, the structural change induced by the adamantyl bridging units produces a looser rotaxane co-conformation that diminishes the ability of the surrounding macrocycle to protect the encapsulated squaraine dye from attack by nucleophiles. In the case of SR molecules with
60 macrocycles containing anthracene sidewalls, there is no obvious change in rotaxane co-conformation. But there is a difference with the corresponding SREP derivative, namely a significantly slower rate of cycloreversion and oxygen release.[13] A series of molecular dynamics (MD) simulations provides reasons for the

Scheme 2 Synthetic schemes and isolated yields.
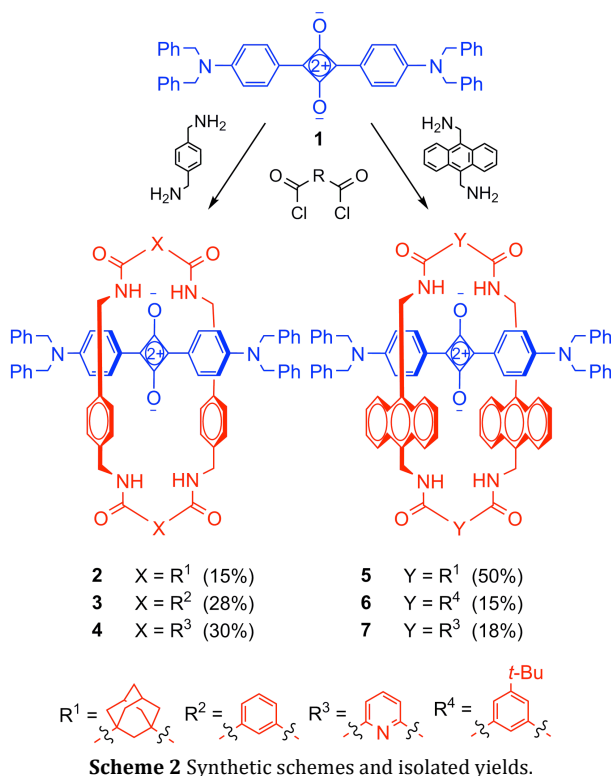
increased co-conformational mobility. Together the results provide new insight and structural methods to control the chemical and photophysical properties of luminescent SR systems.

Results and Discussion

Synthesis

Rotaxanes **2**, **3**, and **4** were prepared by condensing 1,4-bis(aminomethyl)benzene with various dicarbonyl dichlorides in the presence of squaraine **1** (Scheme 2). SR derivatives **3** and **4** were isolated in approximately 30% yield, consistent with previously reported yields for synthesis of phenylene-sidewall SR.[1] The SR **2**, with surrounding macrocycle containing adamantyl bridging units, was susceptible to decomposition during purification and was consequently isolated in a modest 15% yield. Anthracene-sidewall rotaxanes **5**, **6**, and **7** were similarly prepared using a clipping protocol where 9,10-bis(aminomethyl)anthracene was condensed with dicarbonyl dichlorides in the presence of squaraine **1**. The isolated yield for adamantyl-containing SR **5** was excellent (50%) when compared to the 15-18% yields obtained for analogous derivatives **6** and **7**. Additionally, empty anthracene-sidewall macrocycles **9**, **10**, and **11** were prepared for titration experiments by condensing 9,10-bis(aminomethyl)anthracene with the appropriate dicarbonyl dichlorides in the absence of a squaraine template. Interestingly, the empty adamantyl-containing macrocycle **8** could only be isolated in 7% yield, demonstrating the importance of the template effect for increasing the macrocyclization yield.[19, 20]

Anthracene Macrocycle Titrations

The empty anthracene-sidewall tetralactam macrocycles **8**, **9**, and
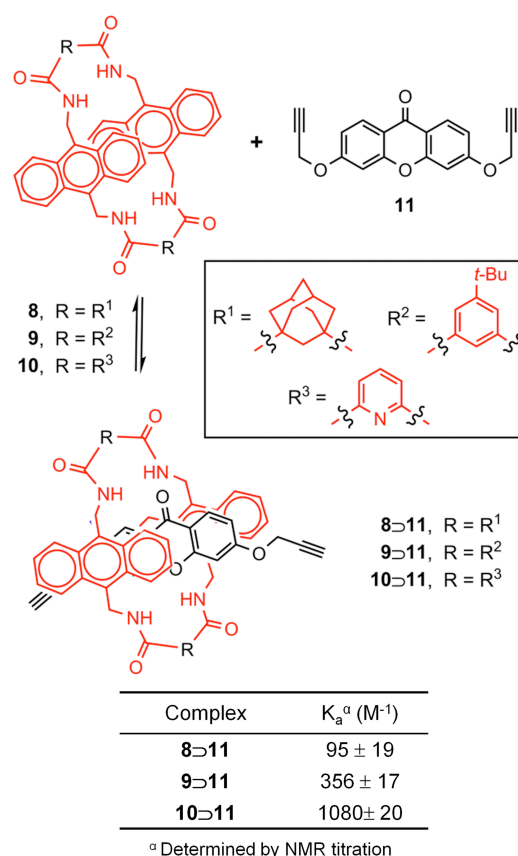

Complex	K_a^α (M^{-1})
8⊃11	95 ± 19
9⊃11	356 ± 17
10⊃11	1080 ± 20

α Determined by NMR titration

Fig. 1 Association constants for tetralactam macrocycles **8-10** with xanthone guest **11** in CDCl$_3$ at 24 °C
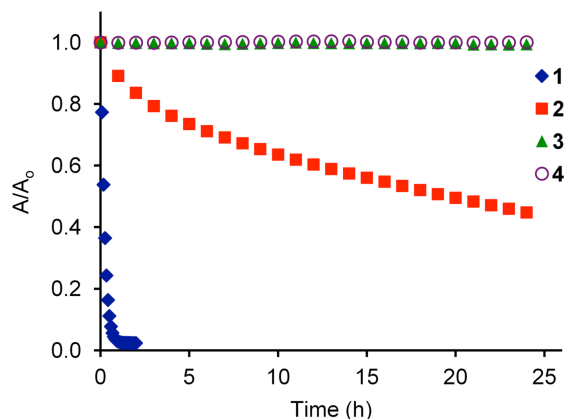

Fig. 2 Comparative chemical stabilities of phenylene-sidewall SR **2-4** and squaraine **1** (each 5.0 μM) in the presence of 2-mercaptoethanol (5.0 mM) in CHCl$_3$. Plots show the change in intensity of the absorption maxima band for each dye at 25 °C

10 are soluble in organic solution (unlike their counterparts with phenylene-sidewalls). This enabled titration experiments with xanthone derivative **11**, a known guest for this macrocycle family (Figure 1).[14] The changes in NMR chemical shift were highly diagnostic for inclusion of **11** inside the macrocycle cavity. Each titration isotherm matched a 1:1 binding model and the derived association constants (K_a) are listed in Figure 1.[21] The data shows that affinity for **11** is in the order **10 > 9 > 8**, which correlates with the relative acidities of the tetralactam NH residues. In other
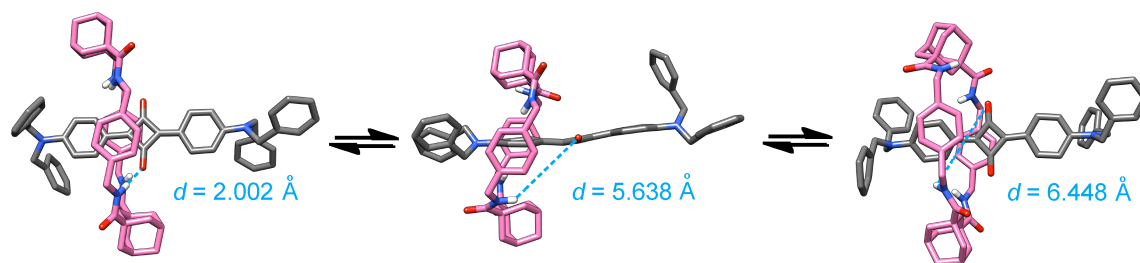
Fig. 3 Three co-conformations from the MD simulation of SR **2** show pirouetting of the macrocycle around the encapsulated squaraine. The length *d* is the distance from one of the macrocycle NH residues to a squaraine oxygen atom

words, the encapsulated guest **11** is held most weakly by the
adamantyl-containing macrocycle **8** with the least acidic NH residues.

Phenylene-Sidewall Rotaxanes

The propensity of SR **2** to decompose under standard silica gel chromatography conditions is very unusual for a SR molecule, and therefore, the chemical stability of **2** was investigated further. Previous studies have shown that squaraine absorption is lost upon nucleophilic attack by thiols.[1] In Figure 2 is a comparison of chromophore stability in the presence of 2-mercapoethanol (5 mM) in CHCl$_3$. As expected, the free squaraine **1** decomposes very quickly, whereas SR **3** and **4** with isophthaloyl and pyridyl bridging units in the surrounding macrocycle are extremely stable. SR **2** with adamantyl bridging units exhibits modest stability, indicating poor steric protection of the encapsulated squaraine by the surrounding macrocycle.

To explain the poor steric protection in SR **2**, we hypothesized that the surrounding macrocycle was relatively mobile with comparatively weak hydrogen bonds to the encapsulated squaraine. This was investigated by conducting MD simulations of SR **2**, **3** and **4.** The MD simulations indicated that the adamantyl-containing macrocycle in **2** pirouettes around the encapsulated squaraine, a feature not observed in the simulation trajectories for rotaxanes **3** and **4** (Figure 3). This pirouetting behavior was quantified by monitoring the length *d* from one of the macrocycle NH residues to a squaraine oxygen atom over the course of the MD simulation (Figure S4 in the ESI). Histograms of these bond distances for SR **2**, **3**, and **4** were plotted, setting bins every 0.1 Å from 0-10 Å
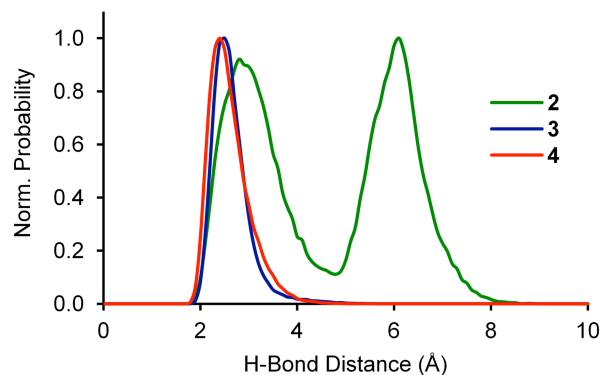

Fig. 4 Normalized histogram of the distance *d* in the MD simulations of phenylene-sidewall SR **2-4**. Two distinct populations are observed for SR **2**, but only a single population exists for **3** and **4**.

(Figure 4). While two distinct populations were observed for SR **2**, only a single population existed for SR **3** and **4** centered near 3 Å. Additionally, the NH•••O angles formed by one of the macrocycle NH residues hydrogen bonded to a squaraine oxygen atom were monitored over the length of the trajectory. As expected, the histogram for SR **2** showed a wider distribution of hydrogen bond angles in comparison to **3** and **4** (Figure S5 in ESI).

A further set of simulations were conducted with added 2-mercaptoethanol molecules (2 μM concentration) to test if MD could explicitly predict the difference in SR susceptibility to nucleophilic attack. The results show that approach of the nucleophilic sulfur in 2-mercaptoethanol to the electrophilic squaraine core is less encumbered in SR **2** than **3** or **4**. While no approaches less than 3 Å were found in any of the simulations (presumably due to insufficient sampling for the detection of these higher energy events), significant differences were found with cutoffs of 4 and 5 Å. The sulfur atom in 2-mercaptoethanol approaches within 4 Å of the core of SR **2**, 19 times more often than in **3** and 9 times more often than in **4**. With a cutoff to 5 Å the 2-mercaptoethanol was 5 times more likely to approach **2** within this distance than in **3** or **4**. The MD results clearly indicate that the SR **2** undergoes an increased number of pirouetting events that expose the core of the encapsulated squaraine to chemical attack.

A final set of calculations tested another reason for the enhanced mobility of the surrounding macrocycle in **2**; namely, the greater torsional flexibility of the adamantyl bridging unit. We hypothesized that conjugation across the 1,3-benzenedicarboxamide or 2,6-pyridinedicarboxamide bridging units restricted dihedral angles and favored macrocycle rigidity. The difference in torsional angle was quantified by scanning the dihedral coordinate at the B3LYP/6-31G* level for two model systems, adamantyl amide and benzamide. The plots in Figure 5 show that dihedral rotation about the conjugated benzamide system is severly hindered in comparison to the adamantyl system. The increased flexibility of the adamantyl bridging unit makes it easier to disrupt a hydrogen bond between the surrounding macrocycle and encapsulated squaraine, leading to enhanced co-conformational mobility.

Anthracene-Sidewall Rotaxanes

Unlike phenylene-sidewall SR **2**, the anthracene-sidewall analogue **6** was chemically stable, suggesting that the surrounding macrocycle with the larger anthracene sidewalls provided greater steric protection of the encapsulated squaraine.
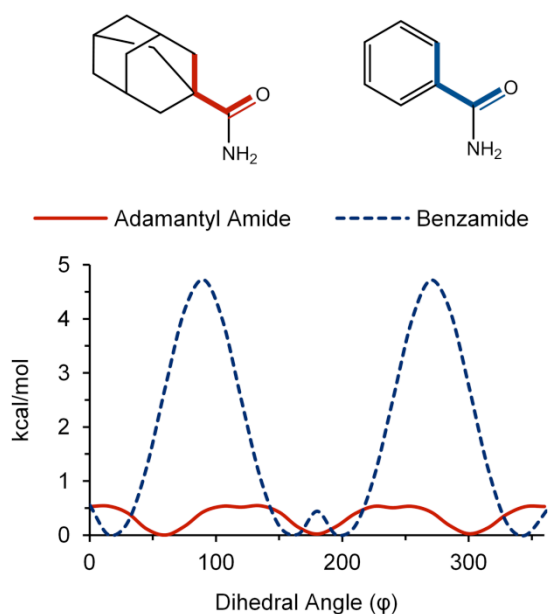
Adamantyl Amide ——— Benzamide - - - -

Fig. 5 Calculated energies for fixed dihedral angles show that the rotation barriers in the adamantyl amide model system are much lower than in the benzamide model system.
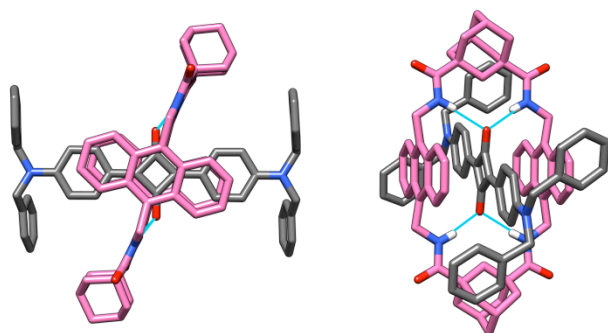

Fig. 6 X-ray crystal structure of SR **5**.

Table 1 Rotaxane Spectral Data

	2	**5**	**6**	**7**
λ_{abs} (nm)	643	659	656[a]	646[a]
λ_{em} (nm)	662	692	689[a]	690[a]
log ε ($M^{-1}cm^{-1}$)	5.33	5.01	5.11[a]	5.03[a]
Φ_f	0.45	0.43	0.48[a]	0.46[a]

[a] Taken from reference 11, [b] Quantum yield measurements (±5 %) were determined in CHCl₃ using 4,4-[bis(*N*,*N*-dimethylamino)phenyl] squaraine dye as a reference ($\Phi_f = 0.70$ in CHCl₃)

Rotaxane	k (h⁻¹)	$t_{1/2}$ (h)	rel. k
5EP	0.06	11	1.0
6EP	0.2[α]	3.2[α]	3.5

[α] Taken from reference 15

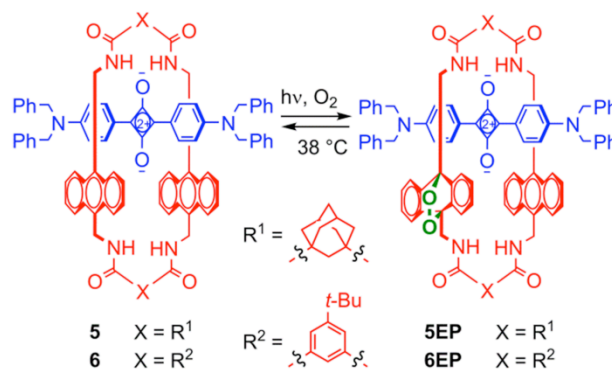**Fig. 7** Rates of SREP cycloreversion in *o*-xylene at 38 °C.

Single crystals of SR **5**, grown by slowly evaporating a chloroform solution, were subjected to synchrotron radiation and X-ray diffraction analysis. The molecular structure was sufficiently resolved to show the macrocycle in a flattened chair conformation with bifurcated hydrogen bonding between the NH residues and the squaraine oxygens (Figure 6). The centroid-to-centroid distance between the two anthracene sidewalls is 6.9 Å, which matches the corresponding distance of 6.91 Å for isophthaloyl-containing SR **6** and is significantly longer than the 6.77 Å for pyridyl-containing **7**. The shorter distance for the pyridyl-containing macrocycle has been discussed before and attributed to macrocycle contraction caused by internal hydrogen bonding of the NH residues with the pyridyl nitrogen.[1] The larger macrocycle cavity sizes in SR **5** and **6** suggest they wrap less tightly around the encapsulated squaraine.

The solution-state ¹H NMR spectrum of SR **5** exhibits diagnostic changes in chemical shift that reflect its interlocked rotaxane structure. The amide protons are shifted downfield from 5.65 to 7.42 ppm, indicative of hydrogen bonding to the squaraine oxygens. The protons on the encapsulated squaraine are shifted upfield due to aromatic anisotropic shielding effects, but

there is no obvious chemical shift trend that discerns any difference in rotaxane co-conformation between **5** and **6**. Similarly, there is no significant difference in the spectral properties for the encapsulated squaraine within these two SR systems (Table 1). Furthermore, anthracene-sidewall SR **5** exhibits the expected 16 nm absorption red-shift when compared to phenylene-sidewall SR **2**.[22] Combined, the structural and spectral data suggests that the surrounding macrocycles in SR **5** and **6** have similar cavity size and degrees of molecular strain.

We have previously shown that irradiation of anthracene-sidewall SR produces a clean photooxidation reaction that generates the corresponding SREP product in nearly quantitative yield. Upon warming, SREPs undergo a cycloreversion process that releases singlet oxygen and emits light. The cavity size of the surrounding macrocycle greatly affects that rate of SREP cycloreversion. Specifically, a SREP derivative with a contracted pyridyl-containing macrocycle is known to undergo greatly accelerated cycloreversion due to enhanced molecular strain on the anthracene-9,10-endoperoxide moiety within the macrocycle.[15] A specific aim of this present study was to evaluate the effect of the adamantyl bridging units on the rate of SREP cycloreversion. Thus, the adamantly-containing endoperoxide **5EP** was prepared in quantitative yield by irradiating an aerated chloroform sample of **5** with red light (Figure 7). Compound **5EP** was stable at low temperature but underwent a chemiluminescent cycloreversion upon warming to 38° C (Figure 8). The rate of **5EP** cycloreversion was determined by monitoring the recovery
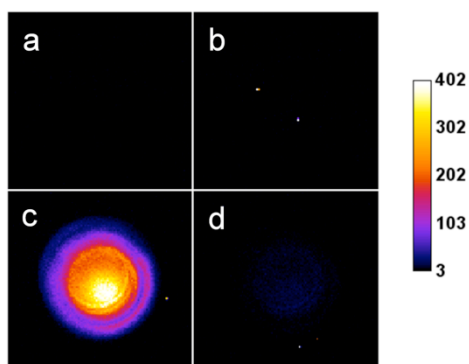
Fig. 8 False colored pixel intensity maps of a vial containing a solution of chemiluminescent **5EP** (200 μL, 1.5 mM in $C_2D_2Cl_4$) warmed to 38 °C. Emission is only observed using the 695–770 nm filter and not in the other three channels, (a) 515–575 nm, (b) 575–650 nm, or (d) 810–875 nm.

of the anthracene absorption band at 374 nm in *o*-xylene. The kinetic plot obeyed first-order rate behavior with k = 0.063 h^{-1} and a half-life of 11 h.[15] This is 3.5 times slower than the cycloreversion rate constant for isophthaloyl-containing **6EP**. The slower cycloreversion of **5EP** is consistent with a decreased amount of cross-component strain between the anthracene-9,10-endoperoxide moiety within the macrocycle and the encapsulated squaraine dye.

Conclusions

SR molecules with surrounding macrocycles containing adamantyl bridging units exhibit higher co-conformational mobility as compared to SR analogues with macrocycles containing isophthaloyl or pyridyl bridging units. This is due to increased torsional flexibility within the 1,3-adamantanediacarboxamide unit and weaker hydrogen bonding to the encapsulated squaraine. In the case of phenylene-sidewall SR **2**, the higher co-conformational mobility leads to increased exposure of the squaraine dye to chemical attack by nucleophiles. Typically, this is an undesired performance feature for fluorescent SR probes. But a potentially useful application of adamantyl-containing tetralactam macrocycles may be within Leigh-type molecular shuttles where they may produce faster shuttling rates.[16] In the case of anthracene-sidewall SR **5**, the adamantyl-containing macrocycle has little effect on chemical or spectral properties. But the corresponding SREP derivative **5EP**, exhibits a slower rate of cycloreversion due to decreased cross-component strain between the anthracene-9,10-endoperoxide moiety within the macrocycle and the encapsulated squaraine dye. The macrocyclic strain in a SREP is structural parameter that can be modified in a systematic way to fine-tune the rate of oxygen release and self-illumination. Combined, the results of this study further show how the structure of the surrounding macrocycle can used to control the chemical and photophysical properties of luminescent SR systems.

Experimental

General Information

Reagents and starting materials were purchased from commercial suppliers and used without further purification. Spectroscopic grade solvents were used for all absorption/emission spectral acquisitions. Thin layer chromatography (TLC) was performed on silica gel 60 F254 (E. Merck). Column chromatography was performed on silica gel (Natland International Corporation, 230-400 mesh) or on SuperFlash Si 35 pre-packed columns (Varian). ^{1}H and ^{13}C NMR spectra were recorded using Varian Unity Plus spectrometers (300, 500, and 600 MHz). Low temperature ^{1}H NMR spectra were recorded using a 600 MHz Varian Unity Plus spectrometer and temperatures were calibrated with a neat methanol (-80 to 10 °C) sample prior to the experimental studies.

Synthesis

Literature compounds **1**,[1] **3**,[1] **4**,[1] **6**,[15] **7**,[15] **9**,[22] **10**,[15] and **11**[14] have been previously reported and were prepared according to published protocols.

SR 2

A solution of 1,3-adamantanedicarbonyl dichloride (65 mg, 0.26 mmol) in anhydrous chloroform (7.0 mL) was drawn up into a 10 mL syringe. A separate solution comprised of 1,4-xylylenediamine (35 mg, 0.26 mmol) and triethylamine (150 mg, 1.40 mmol) in anhydrous chloroform (7.0 mL) was drawn into a separate 10 mL syringe. Over 10 min these solutions were simultaneously added dropwise by a mechanical syringe pump (kd Scientific) apparatus into a stirred solution containing squaraine **1** (10 mg, 0.026 mmol) in anhydrous chloroform (10 mL). Immediately after addition, the reaction was passed through a pad of silica gel and was further washed with 0.5% MeOH/CHCl3 (20 mL). Solvent was removed under reduced pressure and further purification by column chromatography on silica gel with CHCl3 gave SR **2** (20 mg, 15%) as a blue solid. ^{1}H NMR (600 MHz, CDCl3) δ 1.65 (s, 4H), 1.68 (s, 4H), 1.78 (s, 4H), 2.10 (s, 4H), 2.12 (s, 4H), 2.17 (s, 4H), 2.45 (s, 4H), 4.12 (d, *J* = 4.0 Hz, 8H), 4.87 (s, 8H), 6.55 (s, 8H), 6.76 (d, *J* = 9.0 Hz, 4H), 7.23-7.26 (m, 12H), 7.36 (t, *J* = 8.0 Hz, 4H), 7.42 (t, *J* = 7.5 Hz, 8H), 7.87 (d, *J* = 9.0 Hz, 4H); ^{13}C NMR (150 MHz, CDCl3) δ 28.6, 35.6, 39.1, 40.2, 41.9, 44.1, 55.1, 113.3, 119.1, 126.5, 128.4, 129.2, 129.5, 133.6, 135.7, 136.5, 155.3, 178.0, 184.1, 185.8; HRMS (ESI-TOF) calculated for $C_{84}H_{85}N_6O_6$ $[M+H]^+$ 1273.6525; found 1273.6504.

SR 5

A solution of 1,3-adamantanedicarbonyl dichloride (210 mg, 0.80 mmol) in anhydrous chloroform (50 mL) was drawn up into a 100 mL syringe. A separate solution comprised of 9,10-Bis(aminomethyl)anthracene (190 mg, 0.80 mmol) and triethylamine (80 mg, 0.80 mmol) in anhydrous chloroform (50 mL) was drawn into a separate 100 mL syringe. Over 8 h these solutions were simultaneously added dropwise by a mechanical syringe pump (kd Scientific) apparatus into a stirred solution containing squaraine **1** (50 mg, 0.080 mmol) in anhydrous chloroform (50 mL). After stirring overnight, the reaction was filtered through a pad of Celite to remove any polymeric material. Subsequent purification by column chromatography using silica gel with CHCl3 gave SR **5** as a blue-green solid (61 mg, 51 %). ^{1}H NMR (600 MHz, CDCl3) δ 1.68 (s, 4H), 1.70 (s, 4H), 1.89 (s, 4H), 2.23 (s, 4H), 2.27 (s, 4H), 2.30 (s, 4H), 2.51 (s, 4H), 4.86 (s, 8H), 5.00 (d, *J* = 3.5 Hz, 8H), 6.31 (d, *J* = 8.5 Hz, 4H), 6.62 (dd, *J* = 7.0 Hz, *J* = 2.5 Hz, 8H), 7.04 (d, *J* = 8.5 Hz, 4H), 7.32 (d, *J* = 8.0 Hz, 8H), 7.42 (t, *J* = 7.5 Hz, 4H), 7.47-7.52 (m, 12H), 7.63

(dd, J = 6.5 Hz, J = 3.0 Hz, 8H); ^{13}C NMR (150 MHz, CDCl$_3$) δ 28.6, 35.7, 37.4, 39.4, 39.5, 42.1, 55.5, 112.4, 118.4, 124.4, 125.8, 126.6, 128.5, 129.3, 129.5, 130.6, 133.0, 136.3, 154.3, 178.0, 183.2, 184.2; HRMS (ESI-TOF) calculated for C$_{100}$H$_{93}$N$_6$O$_6$ [M+H]$^+$ 1473.7151; found 1473.7178.

5EP

Endoperoxide **5EP** was formed by continual irradiation (150 W Xenon lamp, 520 nm longpass filter) of rotaxane **5** for 90 mins (1-2 mM in CDCl$_3$). Yield was quantitative and no further purification was necessary. **5EP** exists as a blue-green solid. ^{1}H NMR (600 MHz, CDCl$_3$) δ 1.94-2.03 (m, 8H), 2.12-2.17 (m, 12H), 2.36 (s, 4H), 2.58 (s, 4H), 3.98 (d, J = 4.5 Hz, 2H), 4.79 (s, 8H), 5.18 (d, J = 4.5 Hz, 4H), 6.18 (t, J = 4.5 Hz, 2H), 6.40 (d, J = 9.0 Hz, 4H), 6.46 (dd, J = 5.5 Hz, J = 3.0 Hz, 4H), 6.75 (dd, J = 7.0 Hz, J = 3.0 Hz, 4H), 6.93 (dd, J = 5.5 Hz, J = 3.0 Hz, 4H), 7.24 (d, J = 9.0 Hz, 4H), 7.34 (d, J = 7.5 Hz, 8H), 7.42 (t, J = 7.5 Hz, 4H), 7.49 (t, J = 7.5 Hz, 8H), 7.69 (t, J = 4.5 Hz, 2H), 7.85 (dd, J = 7.0 Hz, J = 3.0 Hz, 4H); ^{13}C NMR (150 MHz, CDCl$_3$, 0 °C) δ 183.7, 182.8, 177.9, 177.8, 154.1, 135.8, 135.7, 132.9, 130.0, 129.9, 129.4, 129.2, 128.3, 127.1, 125.1, 124.5, 121.5, 118.7, 112.1, 80.8, 54.3, 42.3, 42.2, 38.9, 38.8, 38.0, 37.5, 36.1, 35.3, 28.3; HRMS (ESI-TOF) calculated for C$_{100}$H$_{93}$N$_6$O$_8$ [M+H]$^+$ 1505.7049; found 1505.7014.

Macrocycle 8

A solution of 1,3-adamantanedicarbonyl dichloride (170 mg, 0.62 mmol) in anhydrous chloroform (50 mL) was drawn up into a 100 mL syringe. A separate solution of 9,10-Bis(aminomethyl)anthracene (140 mg, 0.59 mmol) and triethylamine (700 mg, 7.0 mmol) in anhydrous chloroform (50 mL) was drawn into a separate 100 mL syringe. Over 8 h these solutions were simultaneously added dropwise to a stirred solution of anhydrous chloroform (50 mL). After stirring overnight, the reaction was filtered through a pad of Celite. Macrocycle **8** was obtained after purification by column chromatography using silica gel with MeOH:CHCl$_3$ (1:100) in 7% yield. ^{1}H NMR (500 MHz, CDCl$_3$) δ 1.57-1.60 (m, 4H), 1.63-1.68 (m, 8H), 1.72-1.74 (m, 4H), 2.00-2.05 (m, 8H), 2.18-2.21 (m, 4H), 5.33 (d, J = 5.5 Hz, 8H), 5.65 (t, J = 4.0 Hz, 4H), 7.44 (dd, J = 7.5 Hz, J = 3.0 Hz, 8H), 8.17 (dd, J = 7.0 Hz, J = 3.5 Hz, 8H); ^{13}C NMR data was not obtained due to poor solubility; HRMS (ESI-TOF) calculated for C$_{56}$H$_{57}$N$_4$O$_4$ [M+H]$^+$ 849.4374; found 849.4384.

X-ray diffraction analysis of SR 5

The analysis method and crystallographic data is supplied in the ESI. Additional details for this structure can be found in the crystallographic identification file CCDC-1000259, which can be retrieved from the Cambridge Crystallographic Data Centre via www.ccdc.cam.ac.uk/data_request/cif.

NMR Titrations

^{1}H NMR titrations were performed at 24 °C according to a previously published procedure.[23] A solution of **8**, **9**, or **10** (1.0 mM in CDCl$_3$) was prepared in a NMR tube and initial chemical shifts measured. Aliquots of **11** (20 mM) were titrated into the NMR tube and spectra were acquired after equilibrium had been reached. For all systems, the chemical shift of macrocycle proton '*a*' was monitored. Chemical shift data was plotted and the data was fit via a 1:1 binding model by spreadsheets obtained by K.

Hirose.[21]

Rotaxane Stability

Comparative stabilities of squaraine dye **1** and phenylene-sidewall SR was monitored by the change of the absorption maximum over time. A 5 μM solution of chromophore in CHCl$_3$ was prepared in a screw-capped. 2-Mercaptoethanol (50 mM) was added to the solution and absorption spectra were obtained every 30 minutes over the course of 24 h.

Cycloreversion of 5EP

The cycloreversion rate was determined using a previously published procedure.[24] A solution of **5EP** was prepared in preheated *o*-xylene to give a working concentration of 50 μM within a screw-capped cuvette. The increase in the absorption band at 374 nm was monitored over 60 h.

Molecular Dynamics Simulations

Starting structures of SR analogues **2**, **3**, and **4** were created by modifying structurally-similar crystal structures. Charges for the starting structures were obtained using the GAMESS program.[25] Structures were minimized using the B3LYP/6-31G* level of theory. Electrostatic potentials were subsequently obtained at the HF/6-31G* level. Charges and atom types were then assigned using the *antechamber* module within the AmberTools 12 program. The *xleap* module was used to set up each calculation. The gaff (general Amber force field) force field was used for all MD simulations.

NAMD[26] (version 2.9) was used to perform minimization and MD simulations on both the implicit and explicit solvent models. Pilot simulations utilized the generalized Born implicit solvation model to treat the solvent effects (results not shown for brevity but were comparable to the explicit simulations). A dielectric constant of chloroform (ε = 4.81) was used for the simulations. A cutoff of 20 Å was used for the treatment of non-bonded interactions. Prior to MD simulations, a 1000 step conjugate gradient minimization was performed. 100 nanosecond MD trajectories were obtained for SR **2**, **3**, and **4** using a one femtosecond timestep. The temperature of the system was controlled with a Langevin thermostat set at 300 K. A timestep of 1 femtosecond was used and the output and coordinates were written every picoseconds.

For the explicit solvent calculations, *Packmol*[27] was used to solvate each rotaxane in a box of chloroform. The dimensions of each box is presented in Table S1. Two molecules of 2-mercaptoethanol were added to each system to ensure a 5 μM concentration of 2-mercaptoethanol. Each system was then relaxed by first minimizing the solvent while constraining the solute. This was followed by an unconstrained minimization. Heating to 300 K was performed using an NVT ensemble while constraining the solute. The constraints were then released and 200 nanosecond MD trajectories were obtained for SR **2**, **3**, and **4** using 2 femtosecond timesteps. The SHAKE algorithm was used to constrain bonds between heavy atoms and hydrogen. The output and coordinates were written every picosecond. Histograms of the squaraine-macrocycle hydrogen bond distances were created by setting bins every 0.1 Å from 0-10 Å. In addition, histograms for sulfur-carbon distance vs. time were created by setting bins every 0.1 Å from 0-40 Å. Finally,

histograms for squaraine-macrocycle angle vs. time were created by setting bins every 1 degree from 0-180 degrees. Plots of hydrogen bond distances vs. time were created by extracting the distances every 100 picosecond.

Acknowledgements

Notes and references

a Department of Chemistry and Biochemistry, University of Notre Dame, 236 Nieuwland Science Hall, Notre Dame, IN 46556, USA; Tel:+1-574-631-8632
b Math and Science Department, Concordia University – Portland, 2811 NE Holman Street, Portland, OR 97211, USA; Tel:+1-503-493-6320
* E-mail: smith.115@nd.edu, andjohnson@cu-portland.edu

† Electronic Supplementary Information (ESI) available: Spectral and X-ray crystal data, experimental protocols and additional Figures. See DOI: 10.1039/b000000x/

1. E. Arunkumar, C. C. Forbes, B. C. Noll and B. D. Smith, *J. Am. Chem. Soc.*, 2005, **127**, 3288-3289.
2. J. J. Gassensmith, J. M. Baumes and B. D. Smith, *Chem. Commun.*, 2009, 6329-6338.
3. N. Fu, J. J. Gassensmith and B. D. Smith, *Aust. J. Chem.*, 2010, **63**, 792-796.
4. N. Fu, J. M. Baumes, E. Arunkumar, B. C. Noll and B. D. Smith, *J. Org. Chem.*, 2009, **74**, 6462-6468.
5. E. Arunkumar, N. Fu and B. D. Smith, *Chem.-Eur. J.*, 2006, **12**, 4684-4690.
6. A. G. White, N. Fu, W. M. Leevy, J. J. Lee, M. A. Blasco and B. D. Smith, *Bioconjug. Chem.*, 2010, **21**, 1297-1304.
7. J. J. Lee, A. G. White, D. R. Rice and B. D. Smith, *Chem. Commun.*, 2013, **49**, 3016-3018.
8. J. J. Gassensmith, E. Arunkumar, L. Barr, J. M. Baumes, K. M. DiVittorio, J. R. Johnson, B. C. Noll and B. D. Smith, *J. Am. Chem. Soc.*, 2007, **129**, 15054-15059.
9. E. L. Cole, E. Arunkumar, S. Z. Xiao, B. A. Smith and B. D. Smith, *Org. Biomol. Chem.*, 2012, **10**, 5769-5773.
10. K. M. Harmatys, E. L. Cole and B. D. Smith, *Mol. Pharm.*, 2013, **10**, 4263-4271.
11. J. M. Baumes, J. J. Gassensmith, J. Giblin, J. J. Lee, A. G. White, W. J. Culligan, W. M. Leevy, M. Kuno and B. D. Smith, *Nature Chem.*, 2010, **2**, 1025-1030.
12. C. G. Collins, J. M. Baumes and B. D. Smith, *Chem. Commun.*, 2011, **47**, 12352-12354.
13. C. G. Collins, J. M. Lee, A. G. Oliver, O. Wiest and B. D. Smith, *J. Org. Chem.*, 2014, **79**, 1120-1130.
14. I. Murgu, J. M. Baumes, J. Eberhard, J. J. Gassensmith, E. Arunkumar and B. D. Smith, *J. Org. Chem.*, 2011, **76**, 688-691.
15. J. M. Baumes, I. Murgu, A. Oliver and B. D. Smith, *Org. Lett.*, 2010, **12**, 4980-4983.
16. A. M. Rijs, N. Sandig, M. N. Blom, J. Oomens, J. S. Hannam, D. A. Leigh, F. Zerbetto and W. J. Buma, *Angew. Chem. Int. Ed.*, 2010, **49**, 3896-3900.
17. A. M. Rijs, I. Compagnon, J. Oomens, J. S. Hannam, D. A. Leigh and W. J. Buma, *J. Am. Chem. Soc.*, 2009, **131**, 2428-2429.
18. A. M. Rijs, E. R. Kay, D. A. Leigh and W. J. Buma, *J. Phys. Chem. A*, 2011, **115**, 9669-9675.
19. (a) F. Arico, J. D. Badjic, S. J. Cantrill, A. H. Flood, K. C. F. Leung, Y. Liu and J. F. Stoddart, *Topics Curr. Chem.*, 2005, **249**, 203-259. (b) C. Zhang , S. Li , J. Zhang , K. Zhu , N. Li and F. Huang *Org. Lett.*, 2007, **9**, 5553–5556.
20. T. J. Hubin and D. H. Busch, *Coord. Chem. Rev.*, 2000, **200**, 5-52.
21. K. Hirose, *J. Inclusion Phenom. Macrocyclic Chem.*, 2001, **39**, 193-209.
22. J. J. Gassensmith, L. Barr, J. M. Baumes, A. Paek, A. Nguyen and B. D. Smith, *Org. Lett.*, 2008, **10**, 3343-3346.
23. T. R. Kelly and M. H. Kim, *J. Am. Chem. Soc.*, 1994, **116**, 7072-7080.
24. W. Fudickar and T. Linker, *Chem. Commun.*, 2008, 1771-1773.
25. M. W. Schmidt, K. K. Baldridge, J. A. Boatz, S. T. Elbert, M. S. Gordon, J. H. Jensen, S. Koseki, N. Matsunaga, K. A. Nguyen, S. J. Su, T. L. Windus, M. Dupuis and J. A. Montgomery, *J. Comput. Chem.* 1993, **14**, 1347-1363.
26. J. C. Phillips, R. Braun, W. Wang, J. Gumbart, E. Tajkhorshid, E. Villa, C. Chipot, R. D. Skeel, L. Kale and K. Schulten, *J. Comput. Chem.*, 2005, **26**, 1781-1802.
27. L. Martinez, R. Andrade, E. G. Birgin, J. M. Martinez, *J. Comput. Chem.*, 2009, **13**, 2157-2169.